EXTENDED PDF FORMAT
SPONSORED BY

IMMUNOLOGY2013™ Travel Grants
from R&D Systems
$1000 travel grants will be awarded to
10 immunology researchers
Apply Now!
R&D SYSTEMS
www.rndsystems.com

Three-Dimensional Hydrogen Microscopy in Diamond

P. Reichart *et al.*

Science **306**, 1537 (2004);
DOI: 10.1126/science.1102910

This copy is for your personal, non-commercial use only.

If you wish to distribute this article to others, you can order high-quality copies for your colleagues, clients, or customers by clicking here.

Permission to republish or repurpose articles or portions of articles can be obtained by following the guidelines here.

The following resources related to this article are available online at www.sciencemag.org (this information is current as of January 28, 2013):

Updated information and services, including high-resolution figures, can be found in the online version of this article at:
http://www.sciencemag.org/content/306/5701/1537.full.html

Supporting Online Material can be found at:
http://www.sciencemag.org/content/suppl/2004/11/22/306.5701.1537.DC1.html

This article **cites 30 articles**, 4 of which can be accessed free:
http://www.sciencemag.org/content/306/5701/1537.full.html#ref-list-1

This article has been **cited by** 35 article(s) on the ISI Web of Science

This article has been **cited by** 4 articles hosted by HighWire Press; see:
http://www.sciencemag.org/content/306/5701/1537.full.html#related-urls

This article appears in the following **subject collections:**
Materials Science
http://www.sciencemag.org/cgi/collection/mat_sci

Downloaded from www.sciencemag.org on January 28, 2013

Science (print ISSN 0036-8075; online ISSN 1095-9203) is published weekly, except the last week in December, by the American Association for the Advancement of Science, 1200 New York Avenue NW, Washington, DC 20005. Copyright 2004 by the American Association for the Advancement of Science; all rights reserved. The title *Science* is a registered trademark of AAAS.

15. M. K. J. ter Wiel, R. A. van Delden, A. Meetsma, B. L. Feringa, *J. Am. Chem. Soc.* **125**, 15076 (2003).
16. R. A. van Delden, M. K. J. ter Wiel, H. De Jong, A. Meetsma, B. L. Feringa, *Org. Biomol. Chem.* **2**, 1531 (2004).
17. D. A. Leigh, J. K. Y. Wong, F. Dehez, F. Zerbetto, *Nature* **424**, 174 (2003).
18. P. Reimann, *Phys. Rep.* **361**, 57 (2002).
19. J. M. R. Parrondo, L. Dinís, *Contemp. Phys.* **45**, 147 (2004).
20. R. D. Astumian, *Science* **276**, 917 (1997).
21. Randomizing influences other than Brownian motion can be used in ratchet mechanisms. For example, in quantum ratchets, quantum effects such as tunneling play this role.
22. The principle of detailed balance (*23*) tells us that no net task can be performed by the fluxional exchange of components at equilibrium, because transitions take place at the same rate in opposite directions. The structure of catenane **1** is remarkable in that it separates the kinetic (ability to exchange) and thermodynamic (impetus for net transport) requirements for detailed balance.
23. L. Onsager, *Phys. Rev.* **37**, 405 (1931).
24. R. D. Astumian, P. Hänggi, *Phys. Today* **55**, 33 (November 2002).
25. R. D. Astumian, I. Derényi, *Eur. Biophys. J.* **27**, 474 (1998).
26. Special issue on "Ratchets and Brownian Motors: Basics, Experiments and Applications," H. Linke, Ed., *Appl. Phys. A* **75**, 167 (2002).
27. G. Oster, H. Y. Wang, *Trends Cell Biol.* **13**, 114 (2003).
28. J. Rousselet, L. Salome, A. Ajdari, J. Prost, *Nature* **370**, 446 (1994).
29. L. P. Faucheux, L. S. Bourdieu, P. D. Kaplan, A. J. Libchaber, *Phys. Rev. Lett.* **74**, 1504 (1995).
30. J. S. Bader *et al.*, *Proc. Natl. Acad. Sci. U.S.A.* **96**, 13165 (1999).
31. S. Matthias, F. Müller, *Nature* **424**, 53 (2003).
32. A. Altieri *et al.*, *Angew. Chem. Int. Ed.* **42**, 2296 (2003).
33. The prefix indicates the position of the smaller macrocycle on the larger one.
34. Although catenane *fum-E-***1** was originally prepared as its *O-t*-butyldiphenylsilyl (TBDPS) derivative, the steric bulk caused low yields during the re-silylation protocol of step k, so it was replaced with the smaller TBDMS group for all the directional rotation studies.
35. Materials and methods are available as supporting material on *Science* Online.
36. The photoisomerization reaction gives a 50:50 *E*:*Z* mixture in the photostationary state. No accompanying photodegradation or decomposition was detected (*37*).
37. F. G. Gatti *et al.*, *Proc. Natl. Acad. Sci. U.S.A.* **100**, 10 (2003).
38. By raising or lowering the energy minima, the balance-breaking reactions intrinsically affect the kinetic barriers as well.
39. This is not quite as simple as the ΔG values of the forward and reverse covalent bond forming and breaking reactions canceling each other out. When unlinking takes place, the restriction in freedom of movement reduces the entropy of the small macrocycle in addition to the ΔG change associated with the chemical reaction; however, when linking occurs, the entropy increases by the same amount.
40. Certain aspects of Feynman's discussion of the ratchet and pawl as a motor have been shown to be flawed (*41*, *42*).
41. J. M. R. Parrondo, P. Español, *Am. J. Phys.* **64**, 1125 (1996).
42. M. O. Magnasco, G. Stolovitzky, *J. Stat. Phys.* **93**, 615 (1998).

43. This work was supported by the Carnegie Trust (a scholarship to E.R.K.) and the European Union (a Marie Curie Fellowship to J.V.H.).

Supporting Online Material
www.sciencemag.org/cgi/content/full/306/5701/1532/DC1
Materials and Methods
Scheme S1

11 August 2004; accepted 8 October 2004

Three-Dimensional Hydrogen Microscopy in Diamond

P. Reichart,[1]*† G. Datzmann,[1] A. Hauptner,[1] R. Hertenberger,[2] C. Wild,[3] G. Dollinger[1]‡

A microprobe of protons with an energy of 17 million electron volts is used to quantitatively image three-dimensional hydrogen distributions at a lateral resolution better than 1 micrometer with high sensitivity. Hydrogen images of a <110>-textured undoped polycrystalline diamond film show that most of the hydrogen is located at grain boundaries. The average amount of hydrogen atoms along the grain boundaries is (8.1 ± 1.5) × 10^{14} per square centimeter, corresponding to about a third of a monolayer. The hydrogen content within the grain is below the experimental sensitivity of 1.4 × 10^{16} atoms per cubic centimeter (0.08 atomic parts per million). The data prove a low hydrogen content within chemical vapor deposition–grown diamond and the importance of hydrogen at grain boundaries, for example, with respect to electronic properties of polycrystalline diamond.

Diamond is a promising material for various applications. Although its chemical and mechanical properties have led already to widespread applications, its potential for electronic or optical application remains limited because of imperfections (*1*). The recently demonstrated high carrier mobility in single-crystal chemical vapor–deposited diamond (*2*) opens perspectives for electronic devices in hostile, high-voltage, or high-temperature environments (*3*); diamond optics (*4*); radiation sensors (*5*); and particle detectors (*6*).

However, the production and characterization of high-quality diamond, especially for electronic devices, is a great challenge. Chemical vapor deposition (CVD), for example, is a well-established method (*7*) to synthesize high-quality diamond layers and opens the possibility for hetero- and homo-epitaxial growth of CVD diamond layers up to some mm thickness (*8*, *9*). One main aim is to understand the origin of structural imperfections and impurities and to reduce or control these in order to improve the electronic and optical properties. The presence of hydrogen is known to influence these properties (*10*, *11*). Depending on type and quality, average hydrogen concentrations were found from below the detection limits of 10^{17} atoms/cm^3 up to about 10^{19} atoms/cm^3 in the bulk of polycrystalline diamond layers (*12*). Also, several hydrogen-related complexes were identified (*13*–*15*). However, there is insufficient information about the quantity and the spatial distribution of these, and perhaps as-yet-unidentified, types of hydrogen-related defects. It is even unknown whether most of the hydrogen being detected in diamond is concentrated at grain boundaries, inclusions, and other extended defects or whether hydrogen is distributed homogeneously throughout the bulk at defects of atomic dimensions. The decrease of the hydrogen content with increasing size of the crystallites inside polycrystalline CVD diamond layers, as well as infrared (*15*) or electron spin resonance studies (*16*), indirectly indicate that most of the hydrogen is situated at grain boundaries. Another explanation, however, is that there is reduced defect density within the grains with growing film thickness. Information about the absolute quantity of hydrogen inside the grain compared with

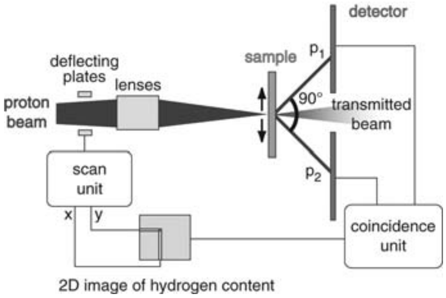

Fig. 1. Hydrogen analysis by pp scattering. The two protons emitted from a proton scattered at a hydrogen nuclei of the sample are detected in coincidence by a suitable detection system (*25*).

---

[1] Physik Department E12, Technische Universität (TU) München, 85748 Garching, Germany. [2] Department für Physik, Ludwig-Maximilians-Universität (LMU) München, 85748 Garching, Germany. [3] Fraunhofer Institut für Angewandte Festköperphysik, 79108 Freiburg, Germany.

*Present address: Microanalytical Research Centre, School of Physics, University of Melbourne, Victoria, 3010, Australia.

†To whom correspondence should be addressed. E-mail: p.reichart@ph.unimelb.edu.au

‡Present address: Angewandte Physik und Messtechnik, Universität der Bundeswehr München, 85577 Neubiberg, Germany.

Fig. 2. (**A**) Surface view of the unpolished polycrystalline CVD diamond sample. (**B**) Cross-sectional image of the original 500-µm-thick polished sample, showing the columnar structure of the diamond layer. Grain sizes increase with distance from the nucleation layer to about 50 µm wide close to the surface. (**C**) Grain structure to clarify the structure of the diamond sample of (B). The dotted line marks the lower surface after polishing the sample from the back in order to perform hydrogen analysis.

those at the grain boundaries is needed to clear this question without doubt.

We concentrate here on the microscopic analysis of hydrogen distributions in CVD diamond. So far, it has been difficult to analyze hydrogen with the necessary sensitivity and lateral resolution to answer this question, despite several attempts to extend existing hydrogen analysis techniques to their limits (*17–19*). Therefore, a method was developed for sensitive three-dimensional hydrogen microscopy (*20*, *21*) by using coincident elastic proton-proton (pp) scattering (*22*). The principle of this technique (Fig. 1) shows that a proton scatters with a hydrogen atom situated inside the sample. The two protons from this elastic pp-scattering reaction leave the scattering site with an angle of 90° to each other. Provided that the scattered protons have enough energy to leave the sample, the coincident detection with this signature is used to filter the pp reaction from all other scattering reactions, and one gets a nearly background-free hydrogen signal. A sensitivity better than 0.1 atomic parts per million (ppm) has been obtained (*23*). This method has been adopted at the proton microprobe SNAKE [superconducting nanoscope for applied nuclear (Kern) physics experiments] (*24*) of the Munich tandem accelerator by using protons with an energy of 17 MeV (*25*). It gives a lateral resolution of better than 1 µm, which is limited by the beam spot size of the microprobe (*23*). Depth information of several-micrometer resolution is obtained simultaneously from energy loss analysis of the scattered protons (*26*).

In order to solve the question on the distribution of hydrogen in diamond, we analyzed a high-quality, polycrystalline, <110>-textured CVD diamond layer (*25*, *27*). The diamond has been deposited in a 6-kW microwave CVD reactor onto a 3-inch Si(100)-wafer at 820°C by using 1% methane in hydrogen gas at 160 mbar. An image of the as-grown surface obtained by optical microscopy (Fig. 2A) shows that the 111 facets of individual grains have an average size of about 50 µm by 50 µm. The cross-sectional view (Fig. 2B) has been taken from the layer that was originally grown to about 500 µm in thickness and mechanically polished at the top surface in order to remove the faceted structure. The columnar crystallites establish from the nucleation layer at the substrate and grow as illustrated (Fig. 2C). As marked with the dotted line, the layer was mechanically polished from the back to get a freestanding sample. The end step of thinning was performed by a reactive ion etching process in oxygen plasma to get a layer 55 µm thick and grain boundaries nearly perpendicular to the surface. The resulting layer is thin enough that the scattered protons from pp scattering can be transmitted through it, and therefore hydrogen imaging becomes possible on that layer. By using atomic force microscopy, we determined a surface roughness of about 0.6 nm (root mean square) on an area of 2 µm by 2 µm.

An optical phase contrast microscope picture of this layer in top view is shown (Fig. 3A) with the grain boundaries clearly visible. The black rectangle marks the 70-µm-long (*x* axis) and 7-µm-wide area (*y* axis) analyzed by the focused 17-MeV proton microbeam with a fluence of 6 × 10^{17} protons/cm^2. The beam dimensions were about 0.6 µm by 2.0 µm at a beam current of 54 pA or 3.4 × 10^8 protons/s. The analysis was performed at room temperature in a hydrocarbon-free scattering chamber at SNAKE at a vacuum pressure of 10^{-7} mbar. No significant change of the hydrogen content at the surface and in the bulk was observed during the analysis (*23*), although a blackening of the irradiation area arose because of defects created by the proton beam in the diamond layer.

The lateral hydrogen distribution as obtained from hydrogen microscopy is superimposed onto the optical image of Fig. 3A. The events from the front or back surface are disregarded in this spectrum in order to reveal the signal from the hydrogen inside the layer. One entry corresponds to about 6.5 × 10^7 H atoms. A sharp accumulation of hydrogen events is visible on the left side, and a broader one on the right, both exactly correlated with the position of the visible structures in the optical image.

A clear view of the hydrogen distribution is given by the cross-sectional hydrogen distribution of the diamond layer (Fig. 3B). The two horizontal branches in the marked areas I-II and III-IV correspond to the hydrogen at the front and back surface of the diamond layer with a content of about (7.2 ± 0.4 ± 1.4) × 10^{15} H atoms/cm^2 and (11.3 ± 0.4 ± 2.2) × 10^{15} H atoms/cm^2, respectively. The first error interval represents the statistical uncertainty; the second represents the systematic uncertainty. Ideal <110> surfaces do not reconstruct (*28*), and one expects about 2.2 × 10^{15} dangling bonds per cm^2 saturated with one hydrogen atom each. The larger hydrogen coverage reflects surface roughness and additional adsorption of water and hydrocarbon molecules as previously proposed (*29*). The widths of the two branches are caused by limited depth resolutions of 3 µm and 6 µm at the upper and lower surface, respectively (*26*). This depth resolution is sufficient to separate the hydrogen-rich surface from the low hydrogen content at depths between the marked points II and III. In Fig. 3B, the two hydrogen enhancements of the superimposed spectrum in Fig. 3A appear localized in lines running between the two surfaces. The left one is nearly perpendicular to the surface, whereas the right one is tilted by about 15° with respect to the surface normal. Therefore, we conclude that the right structure in the optical micrograph of Fig. 3A is a tilted grain boundary. For the left perpendicular grain boundary, the projection of the hydrogen content between II and III to the bottom of the diamond film is shown in Fig. 3C. It depicts a width of the hydrogen enhancement of only 0.6 µm and shows that the principle position resolution is at least as good as this value. The areal density of hydrogen at the grain interfaces is (7.8 ± 1.3 ± 1.6) × 10^{14} H atoms/cm^2 for the left grain

Fig. 3. (**A**) Optical microscopy image of the irradiated diamond sample. With use of the optical phase contrast technique, the grain boundaries become visible. The dark rectangle marks the position of the analyzed area of 70 μm by 7 μm. Superimposed is the lateral distribution of the detected hydrogen events without the hydrogen signal from the surfaces. (**B**) Scatter plot of filtered coincident pp-scattering events calibrated as a two-dimensional cross section of hydrogen distribution. The density of the points scales with the hydrogen content, and one entry corresponds to about 6.5 × 10^7 H atoms. The horizontal branches represent the hydrogen contamination at the surfaces. Corresponding to the position of the grain boundaries in the optical image, two significant enhancements of hydrogen inside the layer are detected. (**C**) The projection of the events in depths between II and III toward the *x* axis in (B) demonstrates the sharpness of the left hydrogen accumulation, showing a principle position resolution better than 0.6 μm.

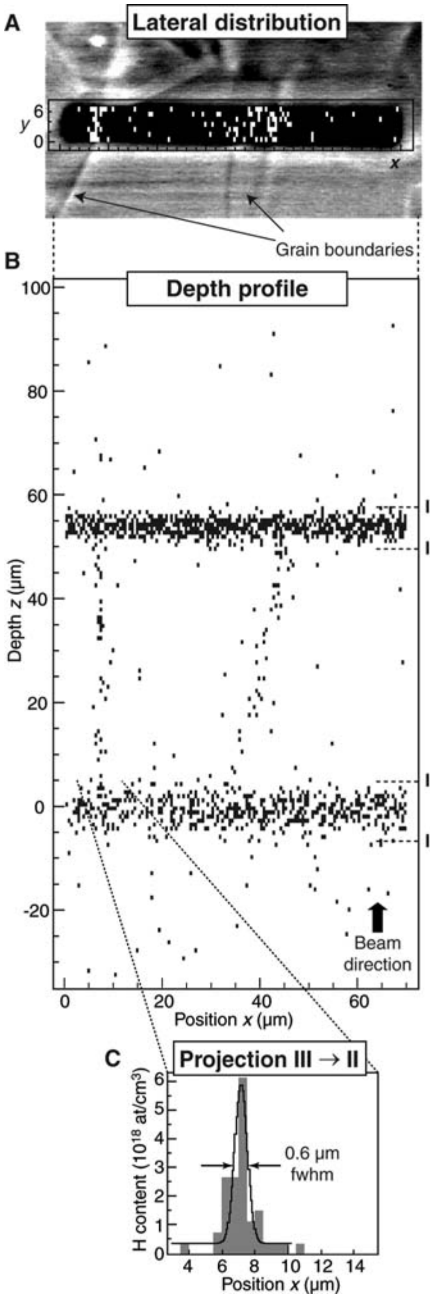

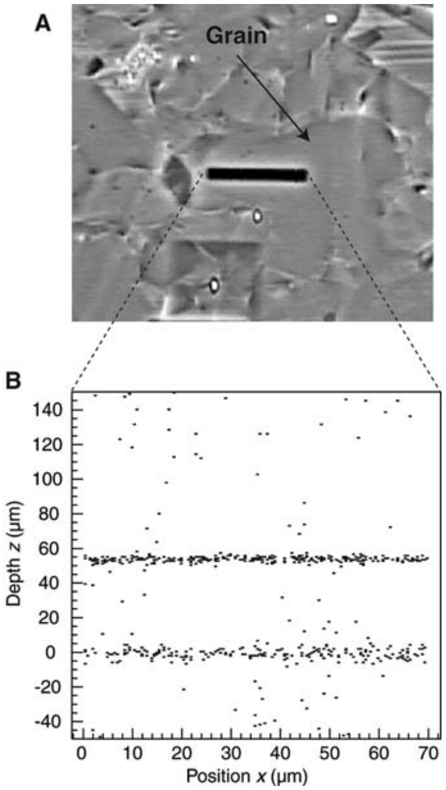

Fig. 4. (**A**) Optical-phase contrast microscopy image of the area around the black marked line scan (70 μm by 7 μm) within a single grain. (**B**) Cross section of the hydrogen distribution as a depth profile, with one event corresponding to 1.0 × 10^8 H atoms. No significant hydrogen enhancement is visible between the branches of the surface hydrogen, and the content is as large as the background by accidental coincidences. This results in an upper limit of 1.2 × 10^{16} H atoms/cm^3 for the hydrogen content within the grain.

boundary and (8.5 ± 1.3 ± 1.7) × 10^{14} H atoms/cm^2 for the right, respectively. This corresponds to about a third of a monolayer of hydrogen situated at each interface between the grains of the polycrystalline layer.

In order to get information on the hydrogen content within the grains, a second measurement has been performed on a single grain. The measured area is marked black in Fig. 4A, which does not contain any visible grain boundary. In accordance, no hydrogen enhancement is visible in the cross-sectional hydrogen distribution (Fig. 4B). One entry in the spectrum corresponds to 1.0 × 10^8 H atoms. Between the hydrogen enhancements at the surface, several counts are present, resulting in ($3.8^{+1.5}_{-1.3}$ ± 0.4) × 10^{16} H atoms/cm^3. However, above the upper and below the lower hydrogen surface layer, a similar density of detected events is visible. These events have to be attributed to accidental coincidence events that are not suppressed by the five-level filter procedure described in (*23*). They give a background level of ($4.2^{+1.5}_{-1.3}$ ± 0.4) × 10^{16} H atoms/cm^3. At this background level, the hydrogen content is consistent with zero and an upper limit of (1.2 ± 0.4) × 10^{16} H atoms/cm^3 with use of the evaluation scheme of Feldman and Cousins at small signals (*30*). In terms of this statistical treatment, the background represents an experimental "sensitivity" of 1.7 × 10^{16} H atoms/cm^3. Taking all measurements made up to now into account, the sensitivity of the microscopic analysis reduces to 1.4 × 10^{16} H atoms/cm^3 (0.08 atomic ppm hydrogen) (*23*).

Our results give further insight into the role of hydrogen with respect to electronic properties of diamond. One expects that the observed hydrogen at the grain boundaries saturates dangling bonds at the grain interfaces and therefore suppresses generation of charge carriers. The hydrogen-containing defects at the grain boundaries probably lead to traps for charge carriers as observed in ion beam–induced current measurements (*31*). At surfaces of some types of diamond, hydrogen bonding is related to p-type surface conductivity (*32*). Several models like the so-called transfer doping model (*33*) are used to describe this conductivity. Similar hydrogen-related doping effects at structural inhomogeneities like the grain interfaces may be proposed for electrical activity inside polycrystalline layers. However, the measured high specific bulk resistance of $\rho > 10^{13}$ ohm·cm of the analyzed sample excludes a doping efficiency similar to that on the diamond surface. This fits with the transfer doping model, because it is conceivable that there would be no suitable molecules within the layer to contribute to the transfer doping process. The low content of hydrogen within the grain proves the potential of microwave CVD to grow high-quality diamond. The content is even well below the doping levels used for p and n doping of diamond and is, therefore, also in line with the high resistance of the studied sample.

References and Notes

1. B. Dischler, C. Wild, Eds., *Low-Pressure Synthetic Diamond*, vol. 11 of *Springer Series in Materials Processing*, W. Michaeli, H. Warlimont, E. Weber, Eds. (Springer, Berlin, 1998).
2. J. Isberg *et al.*, *Science* **297**, 1670 (2002).
3. A. Vescan, I. Daumiller, P. Gluche, W. Ebert, E. Kohn, *Diamond Relat. Mater.* **7**, 581 (1998).
4. E. Wörner, C. Wild, W. Müller-Sebert, P. Koidl, *Diamond Relat. Mater.* **10**, 557 (2001).
5. C. Manfredotti *et al.*, *Nucl. Instrum. Methods* **A458**, 360 (2001).
6. P. Bergonzo *et al.*, *Phys. Status Solidi* (*a*) **185**, 167 (2001).
7. J. C. Angus, C. C. Hayman, *Science* **241**, 913 (1988).
8. H. Kawarada *et al.*, *J. Appl. Phys.* **81**, 3490 (1997).
9. C. Yan, Y. K. Vohra, H. Mao, R. J. Hemley, *Proc. Natl. Acad. Sci. U.S.A.* **99**, 12523 (2002).
10. H. Kawarada, *Surf. Sci. Rep.* **26**, 205 (1996).
11. A. M. Stoneham, in *The Properties of Natural and Synthetic Diamond*, J. E. Field, Ed. (Academic Press, New York, 1992), pp. 4–34.
12. G. Dollinger, A. Bergmaier, C. M. Frey, M. Roesler, H. Verhoeven, *Diamond Relat. Mater.* **4**, 591 (1995).
13. F. Fuchs, C. Wild, K. Schwarz, W. Müller-Sebert, P. Koidl, *Appl. Phys. Lett.* **66**, 177 (1995).
14. C. Glover, M. E. Newton, P. Martineau, D. J. Twitchen, J. M. Baker, *Phys. Rev. Lett.* **90**, 185507 (2003).
15. B. Dischler, C. Wild, W. Müller-Sebert, P. Koidl, *Physica B* **185**, 217 (1993).
16. D. F. Talbot-Ponsonby *et al.*, *Phys. Rev. B* **57**, 2264 (1998).
17. R. D. Maclear *et al.*, *Diamond Relat. Mater.* **8**, 1615 (1999).
18. S. H. Connell *et al.*, *Diamond Relat. Mater.* **7**, 1714 (1998).
19. R. Samlenski, C. Haug, R. Delto, C. Wild, R. Brenn, *Nucl. Instrum. Methods* **B190**, 324 (2002).
20. D. Dujmić, M. Jakšić, N. Soić, T. Tadić, I. Bogdanović, *Nucl. Instrum. Methods* **B111**, 126 (1996).
21. K. A. Sjöland *et al.*, *Nucl. Instrum. Methods* **B124**, 639 (1997).
22. B. L. Cohen, C. L. Fink, J. H. Degnan, *J. Appl. Phys.* **43**, 19 (1972).
23. P. Reichart *et al.*, *Nucl. Instrum. Methods* **B219**, 980 (2004).
24. G. Datzmann *et al.*, *Nucl. Instrum. Methods* **B181**, 20 (2001).
25. Materials and methods are available on *Science* Online.
26. P. Reichart *et al.*, *Nucl. Instrum. Methods* **B197**, 134 (2002).
27. C. Wild, N. Herres, P. Koidl, *J. Appl. Phys.* **68**, 973 (1990).
28. F. Maier *et al.*, *Surf. Sci.* **443**, 177 (1999).
29. A. Bergmaier, G. Dollinger, A. Aleksov, P. Gluche, E. Kohn, *Surf. Sci.* **481**, L433 (2001).
30. G. J. Feldman, R. D. Cousins, *Phys. Rev. D* **57**, 3873 (1998).
31. S. M. Hearne, D. N. Jamieson, E. Trajkov, S. Prawer, J. E. Butler, *Appl. Phys. Lett.* **84**, 4493 (2004).
32. C. E. Nebel *et al.*, *Appl. Phys. Lett.* **79**, 4541 (2001).
33. F. Maier, M. Riedel, B. Mantel, J. Ristein, L. Ley, *Phys. Rev. Lett.* **85**, 3472 (2000).

34. This work was supported by the Beschleunigerlaboratorium der LMU und TU München, as well as the German Bundesministerium für Bildung und Forschung. We thank T. Graf, WSI München, and L. Goergens; TU München, for the atomic force microscopy and x-ray diffraction measurements, as well as M. Schubert, LMU München, and A. Bergmaier; TU München, for data acquisition and programming support. Many thanks also to R. Lutter, O. Schaile, K. Steinberger, LMU Müchen, and the whole accelerator team for their great assistance.

Supporting Online Material
www.sciencemag.org/cgi/content/full/306/5701/1537/DC1
Materials and Methods
Figs. S1 to S5
References and Notes

19 July 2004; accepted 7 October 2004

Probing Electronic Transitions in Individual Carbon Nanotubes by Rayleigh Scattering

Matthew Y. Sfeir,[1]* Feng Wang,[2]* Limin Huang,[3]
Chia-Chin Chuang,[4] J. Hone,[4] Stephen P. O'Brien,[3]
Tony F. Heinz,[2]† Louis E. Brus[1]†

Rayleigh scattering spectra were obtained from individual single-walled carbon nanotubes with the use of a laser-generated visible and near-infrared supercontinuum. This diagnostic method is noninvasive and general for nanoscale objects. The approach permits clear identification of excited states in arbitrary metallic and semiconducting nanotubes. We analyzed spectral lineshapes in relation to the role of excitonic effects and correlated the results with Raman scattering data on individual tubes. The nanotube structure remained the same over distances of tens of micrometers. Small nanotube bundles retained distinct Rayleigh spectroscopic signatures of their component nanotubes, thus allowing the probing of nanotube-nanotube interactions.

Single-walled carbon nanotubes (SWNTs) comprise a family of more than 200 structures characterized by different chiral angles and diameters, each having a distinct electronic structure that can be either metallic or semiconducting (*1*). This richness and diversity, which makes carbon nanotubes so promising for various applications (*2*–*4*), poses a substantial challenge in characterization of specific SWNTs. A general optical characterization technique that permits noninvasive measurements of the electronic structure of an arbitrary individual nanotube has been lacking. Among existing techniques, vibrational spectra of individual SWNTs have been obtained from resonance Raman scattering (*5*–*7*). Although Raman excitation spectra provide some information on the electronic transitions, the requirement of tunable excitation and the weakness of the Raman signal make these experiments extremely challenging (*8*). Recent observations of nanotube fluorescence, and the corresponding excitation spectra, have furthered the characterization of SWNTs (*9*–*11*). However, this approach is inherently limited to semiconducting nanotubes and its application is currently restricted to small-diameter tubes.

We use Rayleigh scattering spectroscopy to identify the electronic transitions of both metallic and semiconducting individual nanotubes. Rayleigh scattering—the ubiquitous process of elastic light scattering from a small, polarizable object—provides spectroscopic information about the system through the scattering resonant enhancement when the photon energy matches that of an electronic transition. Rayleigh scattering occurs whether or not the sample luminesces, and it is intrinsically stronger than inelastic Raman scattering because it does not require the incident light to couple to the vibrations of the system. As such, the approach should be broadly applicable for probing an arbitrary nanoscale object. When implemented with a bright white-light source, the technique offers sufficient versatility and speed to probe spatially localized regions along an individual nanotube, as well as tube-tube interactions in bundles. The method can be easily combined with other types of single-nanotube measurements.

Rayleigh scattering is normally not considered for nanoscale objects because of the expectation that signals will be extremely weak. However, we report that Rayleigh scattering spectra from individual SWNTs can be obtained with high signal-to-noise ratio in less than 1 min with a white-light source of laser brightness. The white-light

---

[1]Department of Chemistry, [2]Departments of Physics and Electrical Engineering, [3]Department of Applied Physics and Applied Mathematics, [4]Department of Mechanical Engineering, Columbia University, 3000 Broadway, New York, NY 10027, USA.

*These authors contributed equally to this work.
†To whom correspondence should be addressed. E-mail: tony.heinz@columbia.edu, leb26@columbia.edu